Available online at www.sciencedirect.com
SCIENCE DIRECT®
Thermochimica Acta 408 (2003) 31–38
thermochimica acta
www.elsevier.com/locate/tca

Observation of multiple phase transitions in n-$C_{22}H_{46}$ using a high resolution and super-sensitive DSC

Shaolan Wang, Ken-ichi Tozaki, Hideko Hayashi, Shotaro Hosaka, Hideaki Inaba*

Department of Science Education, Faculty of Education, Chiba University, 1-33 Yayoi-Chou, Inage-ku, Chiba 263 8522, Japan

Received 19 September 2002; received in revised form 9 May 2003; accepted 16 May 2003

Abstract

The phase transitions of n-$C_{22}H_{46}$ have been measured by using a high resolution and super-sensitive DSC. The crystal–rotator transition and the rotator–melt transition were observed both in the heating and in the cooling run, although a rotator–rotator transition was observed only in the cooling run. A new peak was found at about 3 K above the 'bulk' melting temperature. It is considered to be due to the order–disorder transition of a monolayer on the surface of the liquid alkane. When the cooling rate was below 0.1 mK s^{-1}, the peak due to solidification was separated to give another phase transition.

Keywords: DSC; *n*-Alkane; Phase transition; Surface freezing; Rotator phase

1. Introduction

The normal alkanes CH_3–$(CH_2)_{n-2}$–CH_3 are the most simple organic systems and form the basis of lipids, surfactants, liquid crystals, and polymers. The alkanes have characteristic crystalline phases, which are commonly called rotator phases (R phases), just below their melting points. In these phases, the molecules revolve about their long axes and behave as if they were in a liquid state. Broadhurst [1] found the n-alkanes with $9 \leq n$ (odd) ≤ 39 and with $20 \leq n$ (even) ≤ 38 to have the R phases.

Sirota et al. [2] found five R phases, which are characterized in terms of the molecular tilt, side packing, azimuthal ordering and layer stacking by X-ray scattering study. They [3] also made a calorimetric study of the n-alkanes: C_nH_{2n+2} ($20 \leq n \leq 30$) using an adiabatic scanning calorimeter and found rotator–rotator transitions corresponding to the rotator phases found by the X-ray scattering study [2]. Dynamical structures of the R phases of n-alkanes have also been studied by means of optical observation [4–6], X-ray power diffraction [7–9], photoacoustic and exoelectron emission techniques [10], infrared spectroscopy [11], nuclear magnetic resonance [12–14]. Yamamoto and coworkers [15–17] studied the detailed dynamical structures of the R phases using the molecular simulation method, such as Monte Carlo (MC) and molecular dynamics (MD).

Wu and coworkers [18,19] discovered the surface freezing phenomenon, in which a thin layer at an air/liquid interface crystallizes during cooling at about 3 K higher than the bulk melting point in molten normal alkanes C_nH_{2n+2} ($16 \leq n \leq 50$) using X-ray

* Corresponding author. Tel.: +81-43-290-2599; fax: +81-43-290-2519.
E-mail address: inabah@faculty.chiba-u.jp (H. Inaba).

0040-6031/$ – see front matter © 2003 Elsevier B.V. All rights reserved.
doi:10.1016/S0040-6031(03)00312-5

and surface tension measurements. Yamamoto and coworkers [20–22] investigated this phenomenon using the molecular simulation method. The molecules in the monolayer are hexagonally packed and oriented perpendicular to the surface [18–22]. Yamamoto et al. [23] investigated the surface freezing effect of pentacontane (n-$C_{50}H_{102}$) and tetratetracontane (n-$C_{44}H_{90}$) films evaporated on a copper substrate by differential thermal analysis (DTA) simultaneously with the measurement of surface-specific ultraviolet (UV) photoemission.

Thermal measurement is a powerful tool to obtain thermodynamic information for the phase transitions of n-alkanes. Finke et al. [24] made a calorimetric study of C_nH_{2n+2} ($8 \leq n \leq 16$). They found rotator transitions for C_nH_{2n+2} containing an odd number of carbon atoms and gave enthalpies of the transitions. Barbillon et al. [25] obtained the enthalpies of n-alkanes C_nH_{2n+2} ($18 \leq n \leq 26$) using a differential calorimeter from 260 to 340 K, and found solid-phase transitions. Domanska and Wyrzykowska [26] obtained the heat capacities and enthalpies for the solid–solid transitions and the melting transitions for $C_{22}H_{46}$, $C_{24}H_{50}$, $C_{26}H_{54}$ and $C_{28}H_{58}$ by DSC at a heating rate of 1 K min^{-1}. These measurements, however, are considered to be neither sensitive nor stable enough to detect the fine structure of the rotator transition and to detect the surface freezing phenomenon. The following points may be required to achieve this. The first one is to achieve the enough sensitivity of the apparatus. The second is to measure in both the directions of heating and cooling, since some rotator transitions have thermal hysteresis [2]. The third is to achieve the measurement at a very slow rate of heating and cooling, since the fine structure of the transitions cannot be resolved by a usual scan rate, such as 1 K min^{-1}.

Our research group [27–29] has constructed a high resolution and super-sensitive DSC with a baseline stability of ±3 nW capable of measuring at a very slow scan rate such as 10 μK s^{-1} in both the directions of heating and cooling. One of the driving forces to develop such a high resolution and super-sensitive DSC is to detect a magnetic effect of diamagnetic substances [28,29], which is expected to be very small. We measured the phase transitions of n-$C_{32}H_{66}$ [28], using the calorimeter and observed a new phase transition and several small exothermic subpeaks in the solidifying process and found the magnetic effect on the phase transitions of n-$C_{32}H_{66}$ and EBBA [28,29].

In the present paper, the phase transitions of pure n-$C_{22}H_{46}$ have been measured at very slow heating and cooling rates using a high resolution and super-sensitive DSC, which has been developed by us. The detailed behaviors of the rotator transitions, the different behaviors of the transitions between the heating and the cooling run and the surface freezing phenomenon have been shown and their mechanisms have been discussed.

2. Experimental

2.1. Apparatus

We have improved the high resolution and super-sensitive heat-flux type differential scanning calorimeter in order to obtain a more stable baseline. The schematic drawing of the new home-made high resolution and super-sensitive DSC is shown in Fig. 1. The temperature difference between a test sample and a reference one, produced by a heat absorbed in or released from the sample, was measured by thermoelectric modules, TM1 and TM2, which were made of many semiconducting thermoelectric elements connected in series. The output voltage of each thermoelectric module was about 7.8 mV K^{-1}. Such a high voltage signal for a temperature difference is one of the merits of this calorimeter. The temperature of the sample was measured using a Pt resistance thermometer, TS1, which was regarded as the temperature of the sample. The temperature control of the calorimeter was made two-fold. One was made using a Pt temperature sensor, TS2, by controlling the heater attached at the thick metal vessel. The other was the precise temperature control using a Pt resistance thermometer, TS3, by controlling the current of thermoelectric module, TM3. The measurement can be made in either direction of heating or cooling with this apparatus. The temperature region measurable in the DSC is between 220 and 400 K and the dQ/dt region is from 3 nW to 1 W. The practical region of cooling and heating rate measurable in the DSC is from 1 μK s^{-1} to 10 mK s^{-1}. The calibration of temperature of TS1 was made by measuring the melt point of five kind of standard samples, H_2O, Hg, Ga, $C_{16}H_{32}O_2$ and C_2H_3N. The calibration

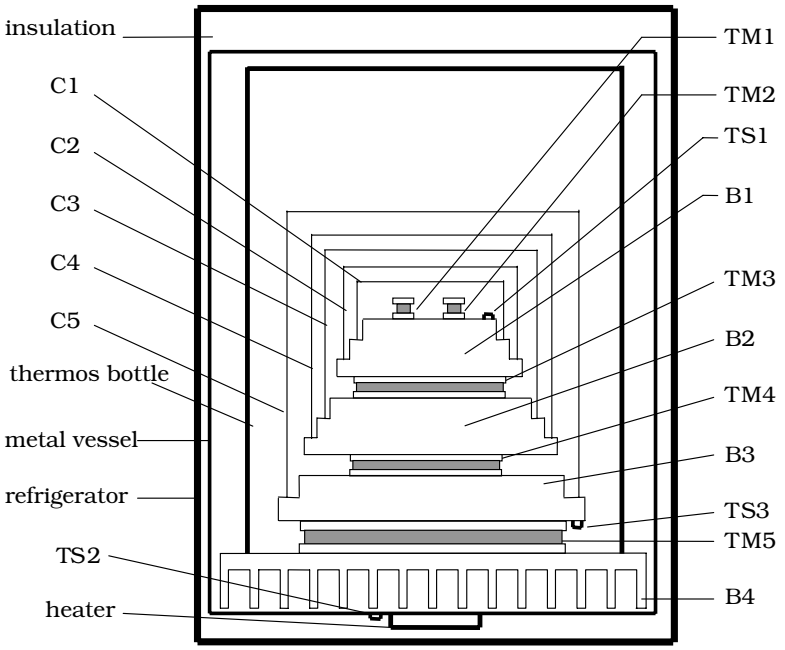

Fig. 1. The schematic drawing of the high resolution and super-sensitive DSC, where TS1–3 are Pt resistance thermometers, C1–5 are copper shields, B1–3 are copper blocks and B4 is an aluminum block.

of energy was made by measuring the specific heat capacity of the standard sample of a single crystalline alumina. The temperature control was within ±0.15 mK and the stability of the baseline was within ±3 nW at 300 K about one order of magnitude better than the previous one [27,28]. This DSC can be used to measure heat capacity. The heat capacity of the alumina was measured within an inaccuracy of 1% [29].

2.2. Sample

The $C_{22}H_{46}$ sample was purchased from National Institute of Standards and Technology (NIST), and its purity was higher than 99.999%. The sample was enclosed in an aluminum capsule for the DSC measurement. The sample amount was 1.28 mg for the cooling rate of 5 μK s^{-1} and 2.48 mg for other heating and cooling rates.

3. Results and discussion

The DSC curve for docosane of the heating run at a rate of 0.5 mK s^{-1} is shown in Fig. 2. We have made these measurements several times and found that the curves are almost the same. We can see two large endothermic peaks centered at 316.22 K (peak 3) and 317.25 K (peak 2) from Fig. 2. Peak 3 is known as

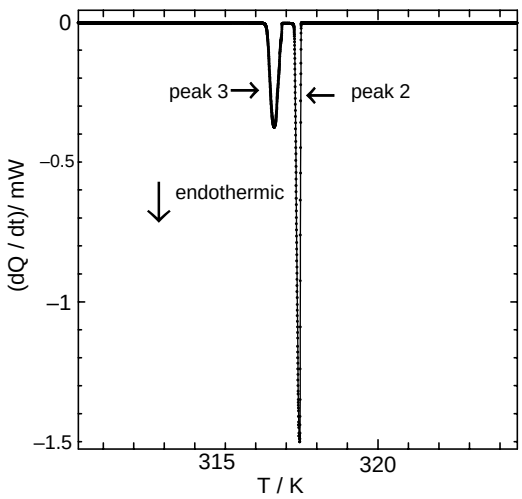

Fig. 2. DSC curve of the heating run at a rate of 0.5 mK s^{-1} of $C_{22}H_{46}$ sample.

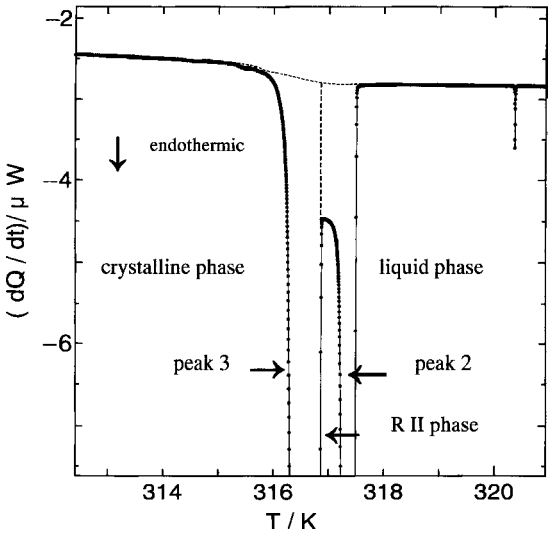

Fig. 3. The magnified DSC curve of the heating run at a rate of 0.5 mK s^{-1} of $C_{22}H_{46}$ sample.

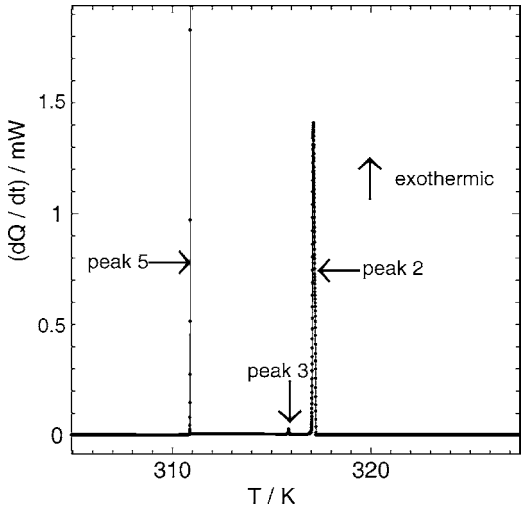

Fig. 4. DSC curve of the cooling run at a rate of 0.5 mK s^{-1} of $C_{22}H_{46}$ sample.

due to the solid–solid transition from the crystalline phase to the rotator phase, and peak 2 is due to the transition from the rotator phase to the liquid phase [2,3,7,25,26,30]. The enthalpy changes of peak 2 and peak 3 were 48.7 and 28.4 kJ mol^{-1}, respectively, in good agreement with the values obtained by Schaerer et al. [30], 48.96 and 28.20 kJ mol^{-1}. The magnified curve of Fig. 2 is shown in Fig. 3, where a new peak (peak 1) is observed around 320.36, 3.11 K above the melting temperature. It is considered to be due to fusion related to the surface freezing phenomenon. The baseline of the heat flux in the liquid phase is about 0.3 μW higher than that in the crystalline phase, which indicates that the heat capacity is different between the crystalline phase and the liquid phase [26]. In contrast with the sharp change of the baseline around 317.5 K in the liquid phase, the gradual rise of the baseline from the crystalline phase to the onset of the rotator phase is observed between 315 and 316 K. This is due to the increase of some fluctuational motions around the C–C bond within the potential minimum in the vicinity of the molecular chain ends in the crystalline phase before the peak 3 is formed [14].

The DSC curve of the cooling run at a rate of 0.5 mK s^{-1} is shown in Fig. 4. We can see two large peaks, peak 5 around 310.95 K and peak 2 around 317.15 K. A very small new peak (peak 3) is observed around 315.95 K besides them. Two rotator phases, the RI and RII are known to exist in $C_{22}H_{46}$ according to Sirota et al. [2,3]. The RI phase has a distorted-hexagonal lattice, where the magnitude of the distortion can be expressed by the order parameter D ($D = 0$ corresponds to the hexagonal (RII) phase). This structure most closely resembles the alkanes of most prevalent low temperature phase (orthorhombic) and has the layers, which are stacked in an AB bilayer stacking sequence. RI phase has been observed only on cooling [2]. On the other hand, RII phase is the phase of highest symmetry. Each layer has an average hexagonal symmetry and the layers are stacked in an ABC trilayer stacking sequence [2,3].

Peak 2 in Fig. 4 is due to the transition from the liquid phase to the rotator phase RII, which is the solidification process. Peak 3 in Fig. 4 is due to the solid–solid transition from the rotator phase RII to the other rotator phase RI. Peak 5 in Fig. 4 is due to the solid–solid transition from the rotator phase RI to the crystalline phase. The magnified curve of Fig. 4 is shown in Fig. 5, where peak 1 at 320.34 K, peak 6 at 307.55 K and a broad exothermic peak (peak 4) in the rotator phases are seen. The enthalpy changes of the peaks are obtained by integrating the area of them and are listed in Tables 1 and 2.

Peaks 1 both on heating shown in Fig. 3 and on cooling shown in Fig. 5 are due to the surface freezing phenomenon. The thermal peak due to the surface

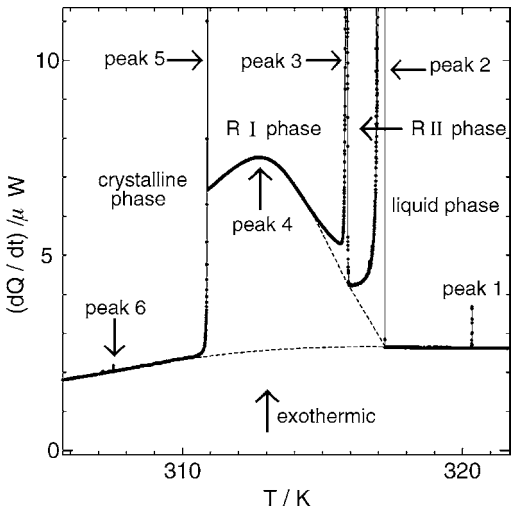

Fig. 5. The magnified DSC curve of the cooling run at a rate of 0.5 mK s^{-1} of $C_{22}H_{46}$ sample.

freezing phenomenon using a bulk sample is detected for the first time, showing the high sensitivity of the calorimeter. Peak 1 detected on heating shown in Fig. 3 is due to the heat absorbed by the fusion of a monolayer formed on the surface of liquid docosane, and peak 1 detected on cooling shown in Fig. 5 is due to the heat generated by the formation of a monolayer on the surface of liquid docosane. The temperature of peak 1 on cooling is 20 mK below that of heating because of super-cooling. The enthalpy change of peak 1 on heating is calculated as 4.4 J mol^{-1}, which is 9.03×10^{-5} times smaller as compared with that of the melting enthalpy obtained from peak 2. On the other hand, the ratio of the molecular number of the surface monolayer to that of the whole sample is calculated as 2.02×10^{-5} using the data of the surface area of the sample in the Al pan, the density [7] and amount of the used sample, and the length of docosane molecule [7], assuming that the molecules form a monolayer on the surface. The fact that the observed ratio of the enthalpy change is about four times larger than the calculated ratio indicates that the ordered phase on the surface of liquid alkane penetrates to the melt. The enthalpy change of peak 1 on cooling is larger than that on heating. This is considered to be due to the phenomenon that some pieces of monolayer is still left after the melting of a monolayer on the surface of liquid alkane on heating.

Table 1
Enthalpy change due to the phase transitions and the ratio to the melting enthalpy of docosane on heating

	Peak 3	Peak 2	Peak 1
T (K)	316.22	317.25	320.36
ΔH (J mol^{-1})	28.4×10^3	48.7×10^3	4.4
Ratio	0.58	1	9.03×10^{-5}

The origin of the broad exothermic peak (peak 4) in the RI phase and RII phase is considered to be related to the rotational action of CH_2 bonds, since it appears at 317.2 K at the beginning of RII phase and suddenly disappears at 311 K at the end of the RI phase in Fig. 5. It may be due to the excited conformational states in the rotator phases. The structural excitation is called as the kink (g^+ tg^-) according to Zoppo and Zerbi [31], which is the combination of one trans and two gauche states of rotating CH_2 bonds. Although the transition becomes significant after the solid–solid transition from the rotator phase RII to the rotator phase RI in the cooling process, it is considered to start with the transition at 317.15 K from the liquid phase to RII phase. The estimated transitional range of the excited conformational states is shown using dotted lines in Fig. 5. It is considered that there is about one kink per one molecular chain as an average judging from the kink energy, 4–6 kJ mol^{-1} [32] and the enthalpy change of peak 4, 5.9 kJ mol^{-1}, as given in Table 2. The location of the kink in the molecular chain would be different from molecule to molecule because of the interaction among them. The concentration of the kink gradually decreases while cooling

Table 2
Enthalpy change due to the phase transitions and the ratio to the solidification enthalpy of docosane on cooling

	Peak 1	Peak 2	Peak 3	Peak 4	Peak 5	Peak 6
T (K)	320.34	317.15	315.95	312.90	310.95	307.55
ΔH (J mol^{-1})	4.6	48.7×10^3	0.36×10^3	5.9×10^3	9.8×10^3	0.24
Ratio	9.45×10^{-5}	1	8.21×10^{-3}	0.12	0.20	4.93×10^{-6}

and then suddenly disappears at the transition from RI phase to the crystalline phase.

The enthalpy change of peak 6 shown in Table 2 is very small. It is 5.22×10^{-2} times smaller as compared with that of the formation enthalpy of a monolayer on the surface of liquid docosane obtained from peak 1. Therefore, peak 6 would be considered as the heat generated by the solidification of rotation of the molecular chain ends of the surface monolayer on the crystalline of docosane, after transition from rotator phase RI to crystalline phase.

Peak 3 detected on cooling, which is shown in Fig. 5 is due to the heat generated by the transition from the rotator phase RII to RI, where the structures are ABC trilayer stacking sequence and AB bilayer one, respectively. The magnitude of the enthalpy of peak 3 shown in Table 2 is only $360\,\mathrm{J\,mol^{-1}}$. It is 7.39×10^{-3} times smaller as compared with that of the solidification enthalpy obtained from peak 2, and just only one-seventh of the thermal energy, at that temperature, RT. This fact suggests that the displacement of molecules through the transition is considered to be small, although the geometrical symmetry changes during the transition.

The magnified curves around the melting temperature of DSC curves of the cooling run at a rate of $5\,\mu\mathrm{K\,s^{-1}}$ is shown in Fig. 6, where the transition from liquid phase to the rotator phase RII is separated into two peaks. The enthalpy change of the higher temperature side is $37.1\,\mathrm{kJ\,mol^{-1}}$ and the one of the low temperature side is $5.6\,\mathrm{kJ\,mol^{-1}}$. The total of them is smaller than the enthalpy change of peak 2, which is shown in Table 2. The enthalpy change of peak 3′ is $158.2\,\mathrm{J\,mol^{-1}}$, about 44% of the one of peak 3. It is considered that a new series of rotator–rotator transition is observed here. Since the transition temperatures of peak 2′ and peak 3′ are as same as the ones of peak 2 and peak 3, respectively, the new rotator phases are named as RII′, RII″, and RI′, respectively, in Fig. 6.

Many very sharp anomalies are observed around 317.2 K in addition to the transition from liquid to the rotator phase RII′. Around 317.2 K, the main solidifying process is already accomplished and only grain-boundary regions of each grain are considered to remain disordered, since the sample is not a single crystalline but is made of many grains. During the very slow cooling process, the solid grains intergrow by absorbing other grains, resulting in the spiky exothermic peaks due to the ordered grain-boundary regions.

The magnified curve of Fig. 6 around 317 K is shown in Fig. 7, where many very sharp anomalies are also observed around 317.05 K in addition to the transition from the rotator phase RII′ to the other rotator phase RII″. Around the temperature of 317.05 K, the main transition process is already accomplished and the RII′ phase is considered to remain only in grain-boundary regions of each grain. During the very slow cooling process, the RII″ grains intergrow by

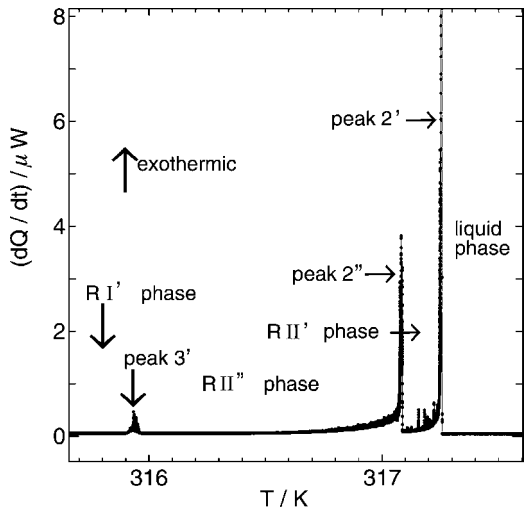

Fig. 6. The magnified DSC curve around melting point of the cooling run at a rate of $5\,\mu\mathrm{K\,s^{-1}}$ of $C_{22}H_{46}$ sample.

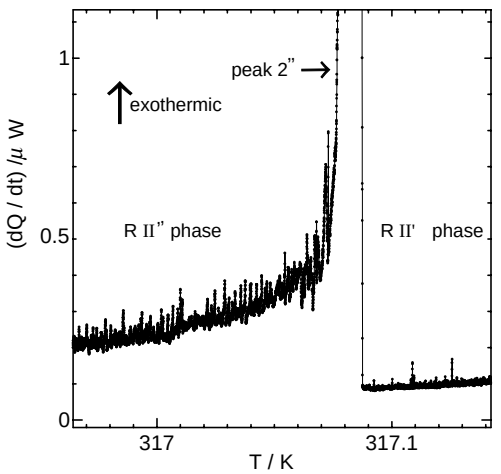

Fig. 7. The magnified DSC curve of Fig. 6 around 317 K.

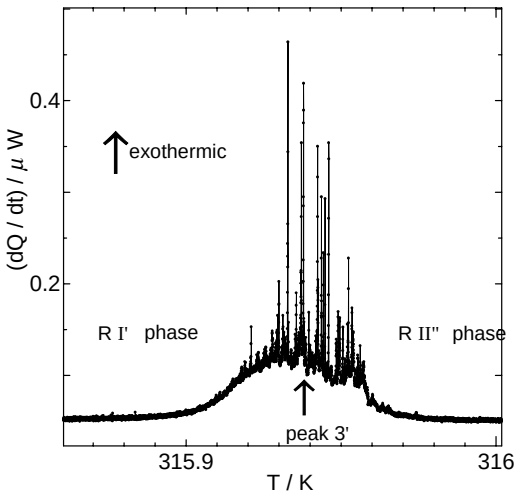

Fig. 8. The magnified DSC curve of Fig. 6 around 315.9 K.

absorbing other grains, resulting in the exothermic peaks due to the more ordered grain-boundary regions.

The magnified curve of Fig. 6 around 315.9 K is shown in Fig. 8. Many spiky exothermic peaks are seen due to the solid–solid transition from RII″ to RI′. The origin of the transition is not known at present, but may be related to the distorted structure of RI phase, which is very sensitive to the order parameter such as the molecular tilt, side packing, azimuthal ordering and layer stacking.

4. Conclusions

The new behaviors of the phase transitions in n-$C_{22}H_{46}$ have been found at the measuring conditions of slow heating and cooling rates using a high resolution and super-sensitive DSC.

(1) The crystal–rotator, the rotator–rotator transition and the melting transition show different behaviors between the heating and the cooling run. In the heating process, the crystalline phase changes into RII phase and then it becomes liquid phase. In the cooling process, the liquid phase changes into RII phase and then changes into RI phase, at last it becomes the crystalline phase.
(2) The peak due to the liquid to RII phase transition is separated into two peaks at a very slow cooling rate, showing a new series of rotator–rotator transition.
(3) A broad peak is observed in the rotator phase in the cooling run. It is interpreted as due to the conformational excitation state such as a kink in the rotator phase.
(4) The formation and disappearance of a monolayer on the surface of liquid alkane is observed about 3 K above the melting temperature using a bulk sample.
(5) A very small new peak is observed at 307.55 K. It is interpreted as due to the solidification of rotation of the molecular chain ends on the surface monolayer in the cooling process.

References

[1] M.G. Broadhurst, J. Res. Natl. Bur. Stand. Sect. A 66 (1962) 241.
[2] E.B. Sirota, H.E. King Jr., D.M. Singer, H.H. Shao, J. Chem. Phys. 98 (7) (1993) 5809.
[3] E.B. Sirota, D.M. Singer, J. Chem. Phys. 101 (12) (1994) 10873.
[4] K. Nozaki, T. Yamamoto, T. Hara, M. Hikosaka, Jpn. J. Appl. Phys. 36 (1997) L146.
[5] K. Nozaki, M. Hikosaka, Jpn. J. Appl. Phys. 37 (1998) 3450.
[6] W. Piesczek, G.R. Strobl, K. Malzahn, Acta Cryst. B 30 (1974) 1278.
[7] I. Denicolo, J. Doucet, A.F. Craievich, J. Chem. Phys. 78 (3) (1983) 1465.
[8] P.B. Shashikanth, P.B.V. Prasad, Ind. J. Eng. Mater. Sci. 7 (2000) 225.
[9] K. Nozaki, N. Higashitani, T. Yamamoto, T. Hara, J. Chem. Phys. 103 (13) (1995) 5762.
[10] T. Gorecki, S.P. Srivastava, G.B. Tiwari, Cz. Gorecki, A. Zurawska, Thermochim. Acta 345 (2000) 25.
[11] Y. Kim, H.L. Strauss, R.G. Snyder, J. Phys. Chem. 93 (1989) 7520.
[12] S. Ishikawa, I. Ando, J. Mol. Struct. 273 (1992) 227.
[13] M.J. Stewart, W.L. Jarrett, L.J. Mathias, R.G. Alamo, L. Mandelkern, Macromolecules 29 (1996) 4963.
[14] R. Kitamaru, F. Horii, M. Nakagawa, K. Takamizawa, Y. Urabe, Y. Ogawa, J. Mol. Struct. 355 (1995) 95.
[15] T. Yamamoto, J. Chem. Phys. 89 (4) (1988) 2356.
[16] T. Yamamoto, J. Chem. Phys. 82 (8) (1985) 3790.
[17] T. Yamamoto, S. Matsumoto, M. Hirose, J. Chem. Phys. 112 (17) (2000) 7627.
[18] B.M. Ocko, X.Z. Wu, E.B. Sirota, S.K. Sinha, O. Gang, M. Deutsch, Phys. Rev. E 55 (1997) 3164.
[19] X.Z. Wu, E.B. Sirota, S.K. Sinha, B.M. Ocko, M. Deutsch, Phys. Rev. Lett. 70 (7) (1993) 958.
[20] H.Z. Li, T. Yamamoto, J. Chem. Phys. 114 (13) (2001) 5774.
[21] T. Shimizu, T. Yamamoto, J. Chem. Phys. 113 (8) (2000) 3351.
[22] M. Kawamata, T. Yamamoto, J. Phys. Soc. Jpn. 66 (1997) 2350.

[23] Y. Yamamoto, H. Ohara, K. Kajikawa, H. Ishii, N. Ueno, K. Seki, Y. Ouchi, Chem. Phys. Lett. 304 (1999) 231.
[24] H.L. Finke, M.E. Gross, G. Waddington, H.M. Huffman, J. Am. Chem. Soc. 76 (1954) 333.
[25] P. Barbillon, L. Schuffenecker, J. Dellacherie, D. Balesdent, M. Dirand, J. Chem. Phys. 88 (1991) 91.
[26] U. Domanska, D. Wyrzykowska, Thermochim. Acta 179 (1991) 265.
[27] K. Tozaki, H. Inaba, H. Hayashi, C. Quan, N. Nemoto, T. Kimura, Thermochim. Acta 397 (2003) 155.
[28] H. Inaba, K. Tozaki, H. Hayashi, C. Quan, N. Nemoto, T. Kimura, Physica B 324 (2002) 63.
[29] S. Hosaka, K. Tozaki, H. Hayashi, H. Inaba, Physica B, in press.
[30] A.A. Schaerer, C.J. Busso, A.E. Smith, L.B. Skinner, J. Am. Chem. Soc. 77 (1955) 2017.
[31] M.D. Zoppo, G. Zerbi, Polymer 33 (1992) 4667.
[32] G.R. Strobl, The Physics of Polymers, Springer, Berlin, 1996.